ACS APPLIED MATERIALS & INTERFACES

Research Article

Cite This: ACS Appl. Mater. Interfaces 2019, 11, 31367−31377

www.acsami.org

# Development of a High-Flux Thin-Film Composite Nanofiltration Membrane with Sub-Nanometer Selectivity Using a pH and Temperature-Responsive Pentablock Co-Polymer

Canbike Bar,[†] Nağahan Çağlar,[†] Metin Uz,[‡] Surya K. Mallapragada,[‡] and Sacide Alsoy Altinkaya*[,†]

[†]Department of Chemical Engineering, Faculty of Engineering, Izmir Institute of Technology, Gulbahce Campus, Urla, Izmir 35430, Turkey

[‡]Department of Chemical and Biological Engineering, Iowa State University, 2114 Sweeney Hall, Ames, Iowa 50011, United States

Supporting Information

**ABSTRACT:** Producing block co-polymer-based nanofiltration (NF) membranes with sharp molecular weight cutoffs via an efficient method exhibiting persistent size-based separation quality is challenging. In this study, this challenge was addressed by reporting a facile approach to fabricate pentablock co-polymer (PBC)-based thin-film composite (TFC) NF membranes. The PBC, consisting of temperature-responsive Pluronic F127 (PEO-*b*-PPO-*b*-PEO) middle blocks and pH-responsive poly(*N*,*N*-(diethylamino)ethyl methacrylate) end blocks, were synthesized by atom-transfer radical polymerization. This polymer was then attached electrostatically to the surface of polysulfone/sulfonated polyether-sulfone support membranes fabricated using a non-solvent-induced phase separation technique. The conformational changes of the PBC chains in response to pH and temperature determined the pure water flux and neutral solute (PEG 1000) rejection performance of TFC membranes. Permeability of the membranes increased from 13.0 ± 0.63 to 15.9 ± 0.06 L/m$^2$·h·bar and from 6.7 ± 0.00 to 13.9 ± 0.07 L/m$^2$·h·bar by changing the solution pH from 4 to 8.5 and temperature from 4 to 25 °C, respectively. The pH- and temperature-responsive conformational changes did not affect the PEG 1000 rejection and membrane pore radius, which remained constant at ∼89% and ∼0.9 nm, respectively. This important finding was attributed to the high grafting density of co-polymer chains, resulting in spatial limitations among the grafted chains. The pore size of ∼0.9 nm achieved with the proposed membrane design is the smallest size reported so far for membranes fabricated from block co-polymers. TFC membranes demonstrated high stability and maintained their flux and rejection values under both static (storage in an acidic solution for up to 1 month) and dynamic (filtering PEG 1000 solution over 1 week) conditions. Pentablock co-polymers enable a NF membrane with a sharp molecular weight cutoff suitable for size-selective separations. The membrane fabrication technique proposed in this study is a scalable and promising alternative that does not involve complex synthetic routes.

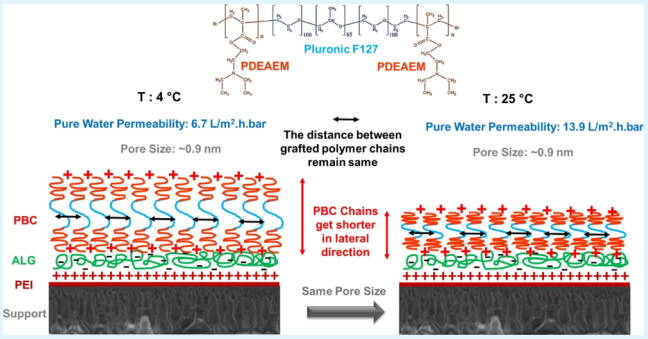


**KEYWORDS:** *Pentablock co-polymer, nanoporous membrane, sub-nanometer pore size, sharp selectivity, nanofiltration, pH and temperature responsiveness*



## INTRODUCTION

In recent years, the application of nanofiltration (NF) membranes in effective separation of different streams has significantly increased. Both charged and uncharged solutes with a molecular weight of less than 1 kDa can be recovered using NF membranes.[1] The recovery of uncharged solutes is more challenging because their rejection is only governed by size exclusion, which is proportional to the ratio between the size of a solute and the pore size of the membrane. An ideal membrane for the separation of small neutral solutes ($M_w$ < 1500) should have a sharp molecular weight cutoff (MWCO), average pore size below 1 nm, low material cost, and persistent stability in the separation performance in the presence of external stimuli.[2]

Recently, block co-polymers have shown promise to manufacture membranes with a narrow pore size distribution.[3−6] However, most membranes prepared from block co-polymers are in the ultrafiltration range with a pore size between 10 and 100 nm.[7−9] Different studies in the literature have been reported to obtain block co-polymer membranes in the NF category. For instance, Yu et al. suggested using mixtures of two chemically interacting co-polymers.[10] They have shown that the resulting membrane is capable of filtering the negatively charged protoporphyrin with a diameter of 1.5

Received: June 12, 2019
Accepted: August 2, 2019
Published: August 19, 2019




DOI: 10.1021/acsami.9b10273
ACS Appl. Mater. Interfaces 2019, 11, 31367−31377

nm. Diep et al. coated anionic and cationic core−shell star block co-polymers on commercial polysulfone (PSf) ultrafiltration supports.[11] Their resulting membrane with 3.5 layers demonstrated NF capability through 98% rejection toward Congo red; however, they did not evaluate the potential of this block co-polymer composite membrane in rejecting neutral solutes. Gu and Wiesner combined additive driven pore expansion with co-polymer chain stretching via charge repulsion to reduce pore sizes from 29 nm at neutral pH down to 5 nm under acidic conditions.[12] Mulvenna et al. reduced pore sizes of polyisoprene-*b*-polystyrene-*b*-poly(*N*,*N*-dimethylacrylamide) (PI−PS−PDMA) membranes from 8 nm to 3.4 nm by converting PDMA lining the pore walls to a poly(acrylic acid)-lined (PAA-lined) structure.[13] They achieved the reduction in pore size through pH-dependent swelling of the chains by raising the pH of the solution from 1 to 4. The common strategy used in these studies to access pore sizes in the NF category is the implementation of weak polyelectrolytes. This approach limits the performance of the membranes to a narrow window of operating conditions. To eliminate the change in the permeability and pore size of the membrane in solutions of varying pH and ionic strength, Zhang et al. attached sulfonic acid moieties onto the pore walls of PI−PS−PAA membranes.[14] Although their pore diameter remained constant at ∼2 nm in the presence of external stimuli, the scale-up possibility of this membrane seems to be difficult. This is because they fabricated the membrane entirely from the block co-polymer using the self-assembly and non-solvent-induced phase inversion technique. The method is suitable for large-scale production; however, block co-polymers are expensive compared to traditional polymers used in water treatment membranes. In order to push block co-polymers into the membrane market, new strategies are needed in developing membranes with a reasonable cost capable of operating reliably over a broad range of operating conditions.

In this work, a versatile strategy was introduced to develop a new thin-film composite (TFC) NF membrane using a pentablock co-polymer (PBC) only in the design of a selective layer. The co-polymer is symmetric and consists of Pluronic F127, poly(ethyleneoxide)-*b*-poly(propyleneoxide)-*b*-poly(ethyleneoxide) (PEO-*b*-PPO-*b*-PEO), as the middle block, and poly(*N*,*N*-(diethylamino)ethyl methacrylate) (PDEAEM) as the end blocks.[15−17] Pluronic F127 exhibits temperature-dependent micellization while tertiary amine groups in methacrylate end blocks show hydrophilic character upon their protonation at low pH and demonstrates various degrees of hydrophobic characteristics above critical pH values where they become deprotonated. By adjusting the co-polymer concentration and coating pH, the chains can be easily attached to the support membrane in brushed conformation (see Scheme 1). At low pH values, the symmetric ends are positively charged. When the co-polymer concentration is sufficiently high, only one end of the co-polymer is attached to the negatively charged support through electrostatic interaction while the other symmetric end becomes free on the surface (see Scheme 1). High grafting densities allow achieving pore radius below 1 nm without any need for multilayer deposition, thermal or chemical post-treatment. In addition, very short distances between the chains due to high grafting density allow the change in chain conformation only in the vertical direction. This enables adjusting the permeability of the membrane using the temperature responsiveness of the co-polymer without changing the pore size. Thus, the TFC membrane (see Scheme 1) provides a means for overcoming permeability-selectivity tradeoff highlighting the key advantage of the PBC used in our study. We report a facile fabrication technique which involves support preparation by the classical phase inversion method from commercially available polymers and dynamic coating of the co-polymer under 1 bar of pressure. The membranes were characterized by scanning electron microscopy (SEM), atomic force microscopy (AFM), X-ray photoelectron spectroscopy (XPS), contact angle, and zeta potential measurements. The influence of pH and temperature on the pure water permeability (PWP), MWCO, and pore size of the membranes was investigated. In addition, the reversibility of the responsiveness and pH stability of the membranes were evaluated. Finally, the long-term stability of the co-polymer layer was tested by measuring the flux and polyethylene glycol (PEG) 1000 rejection continuously. To the best of our knowledge, this is the first study which uses a pH and temperature-responsive PBC in the manufacturing of sub-nanometer size-selective NF membranes.

**Scheme 1. Schematic of the Developed TFC Membrane with the Chemical Formula of Each Component: (a) Pentablock Copolymer, (b) Alginate, (c) Polyethyleneimine, and (d) PSf/Sulfonated Polyethersulfone**

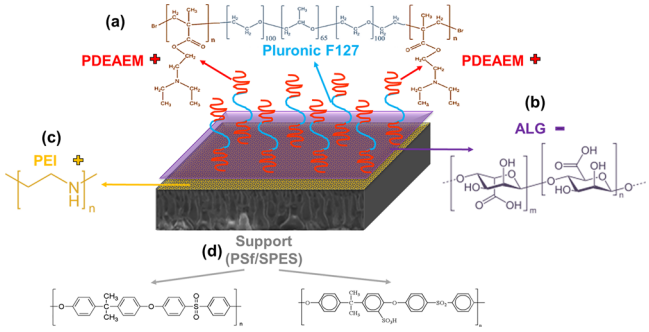


## EXPERIMENTAL SECTION

**Materials.** PSf ($M_w$: 35 kDa), supplied from Sigma-Aldrich Co., and sulfonated polyether sulfone (SPES; $M_w$: 80 kDa) kindly donated by Konishi Chemicals, Japan, were used to prepare the support membrane. Solvents, 1-methyl-2-pyrrolidone (NMP) and *N*,*N*-dimethylacetamide (DMAc) with a purity of >99.5 and >99% respectively, polyelectrolytes, alginic acid sodium salt from brown algae (ALG) (80−120 kDa) and polyethyleneimine (PEI; $M_w$: 25 kDa), and sodium hydroxide (NaOH) in pellets, hydrochloric acid (HCl, 37%), and neutral solutes PEG ($M_w$: 0.6, 1, 6, 10 kDa), glycerol, and sucrose were all purchased from Sigma-Aldrich Co., USA. Polyester nonwoven fabric (05TH-100, thickness: 161 $\mu$m, basis weight: 100 g/m$^2$) was supplied from Hirose Paper Mfg. Co. Ltd.

**PBC Synthesis.** The PBCs were synthesized using atom-transfer radical polymerization (ATRP) following the procedures described previously.[15,17] Briefly, the macroinitiator, difunctional 2-bromo propionate Pluronic F127, was synthesized. Following this, an ATRP reaction was conducted in the presence of a copper catalyst and *N*-propyl-pyridynyl methanimine (*N*-PPM) ligand to attach PDEAEM blocks to the ends of the PluronicF127 initiator. The characterization results for the synthesized co-polymers are shown in Figures S1 through S3 in the Supporting Information.

**Preparation of Porous Support Membrane.** PSf and SPES with a blending ratio of 3:1 were dissolved in a mixture of NMP and DMAc (NMP/DMAc ratio 1:2). The polymer concentration was fixed at 25 wt %. Complete dissolution of the polymers was achieved in 24 h with continuous stirring at 100 rpm. The solution was then cast on a nonwoven support using an automatic film applicator


DOI: 10.1021/acsami.9b10273
ACS Appl. Mater. Interfaces 2019, 11, 31367−31377

(Sheen, Automatic film applicator-1133N, Kingston, England) with a 250 $\mu$m gate size and immediately immersed into a coagulation bath containing 0.5 wt % PEI solution at 25 °C. The membranes were left in the bath for 12 h, washed for ~3 days with deionized water (DI) to remove excess PEI on the surface, and then stored in DI water until filtration tests.

**Preparation of TFC Membrane.** To prepare TFC membranes, positively charged PEI-modified porous support membranes (which will be referred to as "support membrane" in the rest of the text) were first coated with 1 mg/mL of ALG solution at pH 4. For coating, the active surface of the porous support membrane was placed in a dead-end filtration cell (model 8010, Millipore Corp.) and ALG solution was filtered at 1 bar for 15 min. The membrane surface was then rinsed five times and washed with DI water for 5 min to remove loosely bound polyelectrolytes before coating with the PBC. Following rinsing, the DI water whose pH was adjusted to 4 with HCl was filtered through the modified membrane at 2.5 bar until steady state was reached to equilibrate the membrane. Finally, the PBC was coated dynamically at 1 bar by filtering 18 mg/mL of PBC solution at pH 4 for 150 min.

For the determination of grafting density ($\sigma$), both the alginate-modified support and the PBC-coated membranes were dried under room conditions for 48 h and then their weights were measured with an electronic balance (Sartorius CP2P, Germany; max. weighing capacity: 2.1 g; readability: 0.01 mg). The grafting density was then calculated by dividing the difference in the membrane weight before and after PBC coating to the area of the membrane.

**Characterization of Membranes.** SEM, FEI Quanta 250 FEG, was used for observing the cross-sectional morphology of the membranes. The membrane samples were freeze-fractured under liquid nitrogen for cross-sectional imaging. Dried membrane samples were sputter-coated with a gold layer using a Magnetron Sputter Coating Instrument.

AFM analysis was performed both under dry and wet conditions by using a MMSPM Nanoscope 8 from Bruker. Scanning on dry and wet membranes was done in tapping mode for a 5 × 5 $\mu$m surface by using a TAP150 model tip (material: 0.01−0.025 Ω cm antinomy (n) doped Si). AFM images under wet conditions were collected in water at 4 and 25 °C to analyze the temperature responsiveness of the PBC-coated membrane. In addition, the thickness of the swollen PBC layer on the silicon wafer was also measured at 4 and 25 °C using a Mprobe-Vis20 reflectometer system with a spectral range of 450−1000 nm.

The hydrophilic character of the uncoated and PBC-coated TFC membranes was determined with static water contact angle measurements using Attention Optical Tensiometer. Prior to analysis, the membranes were dried for 24 h at room temperature to remove the moisture. Measurements were taken at 4 and 25 °C with DI water (drop volume 5 $\mu$L) at different pH values [pH 4 (<p$K_a$ of the PBC), pH 7.6 (=p$K_a$ of the PBC), and pH 8.5 (>p$K_a$ of the PBC)]. The PBC used in this study exhibit a pH-sensitive behavior by changing their conformation significantly with changes in solution pH as demonstrated in our previous studies.[15−17] The pendant tertiary amine groups of the methacrylate blocks are weakly basic, which makes the copolymer electrostatically charged and hydrophilic at low pH and relatively hydrophobic at higher pH values. Our previous studies estimated the critical pH value at which the pendant amines become uncharged as 7.6 through potentiometric titration, nuclear magnetic resonance (NMR), and quasielastic light scattering (QELS) measurements. At low pH values (pH 4), electrostatic interactions between the charged groups along the copolymer chain likely result in extended chain conformations, while uncharged methacrylate blocks most likely exist in a more compact conformation at high pH (pH 8.5). NMR results indicated the dehydration and reduced mobility of the PDEAEM blocks as they become deprotonated and as the PDEAEM blocks change from hydrophilic polyelectrolytes to uncharged hydrophobic blocks, upon increasing pH.[15−17] QELS measurements showed that the hydrodynamic radii (Rh) of pentablock copolymer micelles increased as a function of pH.[15−17] On the basis of these previous findings, we selected pH 4, 7.6, and 8.5 to observe the effect of conformational changes on the membrane performance. The lower critical solution temperature (LCST) of the PBC was determined as ~20 °C.[16,17] To investigate the temperature responsiveness of the copolymer, the membrane performance was tested above (at 25 °C) and below (at 4 °C) the LCST.

Zeta potential measurements were carried out in the presence of 10 mM NaCl solution with a NanoPlus Micromeritics Instrument. The pH value of the electrolyte solution was adjusted using HCl for acidic pH and NaOH for basic pH.

The presence of a PBC layer on the support membrane was determined with XPS analysis by Thermo Scientific K-Alpha with an electron takeoff angle of 45° to the sample plane.

**Water Flux and Rejection Measurements.** Water flux and rejection tests were carried out using a dead-end cell filtration system (Model 8010, Millipore Corp.) with a total internal volume of 10 mL and an active surface area of 4.1 cm$^2$. Each membrane was first compacted at 2.5 bar until steady state is attained, after which the cell was filled with DI water and permeate was collected at 2 bar. Pure water flux ($J_w$) and PWP were calculated from volume versus time data using eqs 1 and 2.

$$J_w = \left(\frac{\Delta V}{A \times \Delta t}\right) \tag{1}$$

$$\mathrm{PWP} = \left(\frac{\Delta V}{A \times \Delta t \times \Delta P}\right) \tag{2}$$

Filtration of model solutes was carried out in the same dead-end filtration cell system as described above. Before each rejection test, pure water filtration was carried out. Neutral solutes, PEG 1000, PEG 600, sucrose ($M_w$: 342 Da), glucose ($M_w$: 180 Da), and glycerol ($M_w$: 92 Da), were dissolved in DI water to prepare a 1 g/L of concentration, and pH was adjusted with either NaOH or HCl. The solution (10 mL) was filtered at 2 bar until 5 mL of permeate was collected. This procedure was repeated three times with fresh solution under the same conditions to ensure that the membrane is fully conditioned with each solute. The concentrations of solutes in the feed solution ($C_f$), permeate ($C_p$), and retentate ($C_r$) were determined using a Rudolph—J357 Automatic Refractometer. The rejection was then calculated by using eq 3.

$$R(\%) = \left(1 - \frac{C_p}{C_{Bulk}}\right) \times 100 \tag{3}$$

The bulk concentration, $C_{Bulk}$, was calculated from the arithmetic average of the concentrations measured at the beginning ($C_f$) and at the end of the rejection experiment ($C_r$) to take the change in concentration on the feed side into account.

**Average Pore Size Determination.** The influences of pH and temperature on the pore sizes of the membrane were quantified by determining the rejection of model neutral solutes by the membranes. The pore sizes were evaluated by combining experimentally measured rejection data with eq 4 through 8.[18,19]

$$R = 1 - \frac{C_p}{C_{Bulk}} = 1 - \frac{K_{i,c}\Phi}{1 - \exp(-Pe_m)[1 - \Phi K_{i,c}]} \tag{4}$$

$$Pe_m = \frac{K_{i,c}}{K_{i,d}}\frac{VL}{D_{i,\infty}A} \qquad \Phi = (1-\lambda)^2 \qquad \lambda = \frac{r_s}{r_p} \tag{5}$$

$$K_{i,d} = K^{-1}(\lambda, 0) \qquad K_{i,c} = (2 - \Phi)G(\lambda, 0) \tag{6}$$

$$K^{-1} = 1 - 2.401\,\lambda + 1.153\,\lambda^2 - 0.118\,\lambda^3 \tag{7}$$

$$G(\lambda, 0) = 1 + 0.042\,\lambda - 0.941\,\lambda^2 + 0.339\,\lambda^3 \tag{8}$$

In these equations, $V$ is the filtration rate, $L$ and $A$ are the membrane thickness and porosity, $D_{i,\infty}$ is the solute diffusivity in solution, and $r_s$ and $r_p$ are the solute and pore sizes, respectively.

The pore radius distribution of the membranes was calculated using the probability density function based on the assumption of no



DOI: 10.1021/acsami.9b10273
ACS Appl. Mater. Interfaces 2019, 11, 31367−31377

interaction (steric and hydrodynamic) between the neutral PEG molecules and pores of the membranes (eq 9).[20]

$$\frac{dR(r_p)}{dr_p} = \frac{1}{r_p \times \ln \sigma_p \times \sqrt{2\pi}} \exp\left[-\frac{(\ln r_p - \ln \mu_p)^2}{2 \times (\ln \sigma_p)^2}\right] \quad (9)$$

where $\mu_p$ is the mean effective pore radius determined at the PEG rejection coefficient of 50% and $\sigma_p$ is the geometric standard deviation defined as the ratio of radius $r_p$ at the PEG rejection of 83.14% over that at 50%.

**Stability Test.** The stability of the layers on the membrane surface was investigated by storing the membrane in DI water adjusted to different pH values [pH 4 (<p$K_a$ of the PBC), pH 7.6 (=p$K_a$ of the PBC), and pH 8.5 (>p$K_a$ of the PBC)] under static conditions. The PWP and PEG 1000 rejection of the membranes were measured at the end of 7, 14, and 30 days of storage in DI water at each aforementioned pH values. In addition, the rejection and the flux of the PEG 1000 solution during filtration in a cross-flow unit were followed over 1 week.

## RESULTS AND DISCUSSION

**Morphology and Surface Properties of the Membranes.** We first prepared the support of the TFC membrane from a blend of PSf and SPES using DI water as the coagulation medium. The PBC was then directly attached to the surface of this support membrane through electrostatic interactions between negatively charged $SO_3^-$ groups of the SPES and positively charged tertiary amine groups of the PBC. The resulting PBC-coated membrane had less than 50% PEG 1000 rejection. Changing the casting or coagulation bath composition by adding surfactant into water did not significantly increase the rejection. As a next strategy, we added a large molecular weight additive, 25 kDa PEI (0.5 wt %), into the coagulation bath and then coated the support membrane with alginate before electrostatically attaching the PBC to the ALG layer. Combined effects of the delayed precipitation during support preparation due to presence of PEI in the coagulation bath and alginate coating on the support resulted in an increase in the PEG 1000 rejection from 50 to ~89%.

Table 1 lists the zeta potential of the support and PBC-coated membranes. The net charge of the support membrane at three pH values was found positive, which simply confirmed the presence of PEI in the support. During coagulation, PEI diffuses into the polymer solution and attaches to the $SO_3^-$ groups in the SPES through ionic bonding. Among the three pH values investigated, the support membrane displayed the highest zeta potential at pH 4 because of the protonated amine groups in the PEI structure, and its surface charge densities at pH 7.6 and 8.5 are not statistically different from each other, considering the standard deviations of the measurements (Table 1). This can be attributed to the fact that the deprotonation/protonation rate is the same within the pH range of 7−9 as indicated in other studies.[21] The zeta potential of the PBC-coated membrane decreased gradually during the increase of pH from 4 to 8.5 due to deprotonation of the pendant tertiary amine groups of the methacrylate blocks in the PBC as demonstrated in our previous studies.[15−17]

**Table 1. Zeta Potential Data for the Support and PBC-Coated TFC Membranes**

| | zeta potential (mV) | | |
|---|---|---|---|
| membrane code | pH: 4 | pH: 7.6 | pH: 8.5 |
| support membrane | 14.07 + 072 | 6.40 + 0.68 | 7.10 + 0.47 |
| PBC-coated TFC membrane | 8.35 + 0.69 | 5.93 + 0.0 | 4.68 + 0.48 |

Figure 1a,b illustrates the XPS survey scans of the support and TFC membranes. The results show that both membranes primarily contain carbon, oxygen, and nitrogen elements. The intensity of O (1s) in the TFC membrane increased significantly compared to that of the support membrane. Additional oxygen elements in the coated layer come both from alginate and the PBC. The ratios of elemental compositions determined from XPS scans are listed in Figure 1c. According to the results, the absence of sulfur element in the TFC membrane and the decrease in C 1s/N 1s and C 1s/O 1s ratios in the TFC membrane compared to corresponding values in the support membrane are clear indication of successful coating.

Further information about the presence of PBC layer was obtained by deconvolution of C (1s) high-resolution XPS spectra as shown in Figure 1d,e for the support and the PBC-coated TFC membranes, respectively. The C 1s spectrum of the support membrane contains major peaks at a binding energy (BE) of 284.49, 285.57, and 286.53 eV, which are assigned to C−C, C−N, and C−O−C bonds, respectively.[22] A new peak shown in Figure 1e at BE 288.79 eV which is attributed to O═C−O in the PBC[23] demonstrates the successful PBC coating. The O 1s spectra of the support and PBC-coated membranes are shown in Figure 1f,g. The O 1s spectrum of the support membrane has a peak at BE 531.09 eV,[24] which is attributed to the contribution of oxygen in the sulfone. The absence of this peak and the appearance of a new peak at BE 532.66 eV[22] in Figure 1g attributed to O−C═O imply the PBC coating on the support.

Figure 2a,b illustrates the SEM images of the support and TFC membranes. As can be seen in the images, the coating did not distort the bulk structure of the support membrane. Although both membranes displayed similar finger-like pores in the sublayer, the thickness of the dense layer at the top surface increased through PBC coating. Using Image J software, the total and dense skin layer thicknesses were determined as 46.4 ± 2.6 $\mu$m and 0.58 ± 0.038 $\mu$m versus 52.9 ± 1.7 $\mu$m and 1.16 ± 0.17 $\mu$m for the support and PBC-coated membranes, respectively. The thickness of the PBC-coated layer was then estimated to be 6.5 $\mu$m. The measured coating layer thickness was found in agreement with the value calculated by dividing the grafting density (0.75 mg/cm$^2$) to the density of the PBC (1.1 g/cm$^3$). The AFM images shown in Figure 2c,d have shown that the PBC coating resulted in a significant decrease in surface roughness from 24.8 ± 1.16 to 9.79 ± 0.37 nm. In the support membrane, SPES and PEI are ionically bonded to each other and free PSf causes a relatively rough surface. On the other hand, strong electrostatic interactions between the PBC and the ALG-modified support decreased the roughness of the support membrane.

Our membrane design included pH-responsive chains in the support, alginate, and PBC layers. To evaluate the responsiveness of each layer, first, the PWP and PEG 1000 rejection of the support and ALG-modified support membranes were measured at pH 4 (<p$K_a$ of the PBC) and pH 8.5 (>p$K_a$ of the PBC) and the results are shown in Figure 3.

Both the permeability and rejection ability of the support membrane increased by 15 and 34%, respectively, when pH was raised from 4 to 8.5. This could be attributed to two factors. First, the hydrophilicity of the surface was enhanced as


DOI: 10.1021/acsami.9b10273
ACS Appl. Mater. Interfaces 2019, 11, 31367−31377

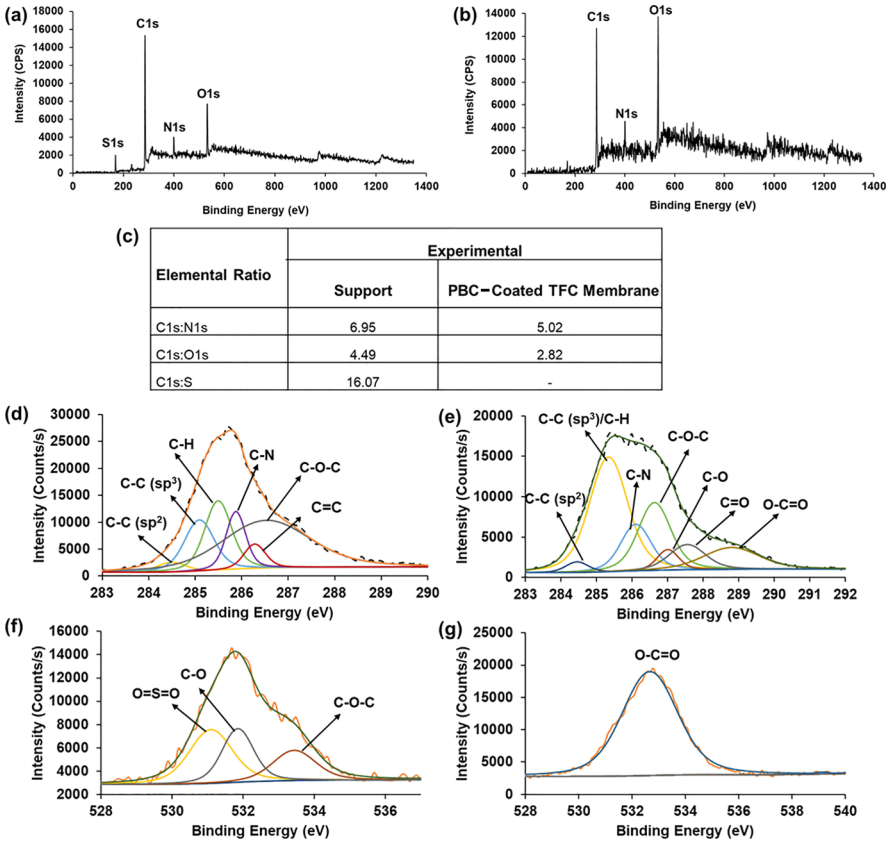


| (c) Elemental Ratio | Experimental | |
|---|---|---|
| | Support | PBC−Coated TFC Membrane |
| C1s:N1s | 6.95 | 5.02 |
| C1s:O1s | 4.49 | 2.82 |
| C1s:S | 16.07 | - |

**Figure 1.** XPS spectrum of (a) support membrane and (b) PBC-coated TFC membrane. Scanning angle 45°. (c) Elemental ratios calculated from XPS spectra. Convoluted high-resolution C (1s) spectra for (d) support and (e) PBC-coated membrane. Convoluted high-resolution O (1s) spectra for (f) support and (g) PBC-coated membrane.

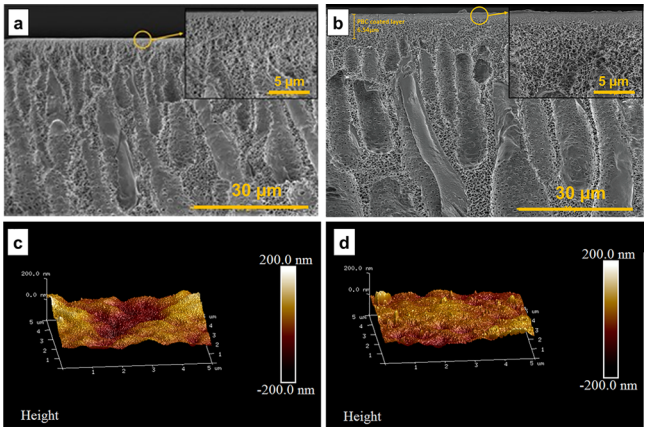


**Figure 2.** Cross-sectional SEM images of (a) support membrane and (b) PBC-coated TFC membrane (magnification 5000×). AFM images of (c) support membrane and (d) PBC-coated TFC membrane.

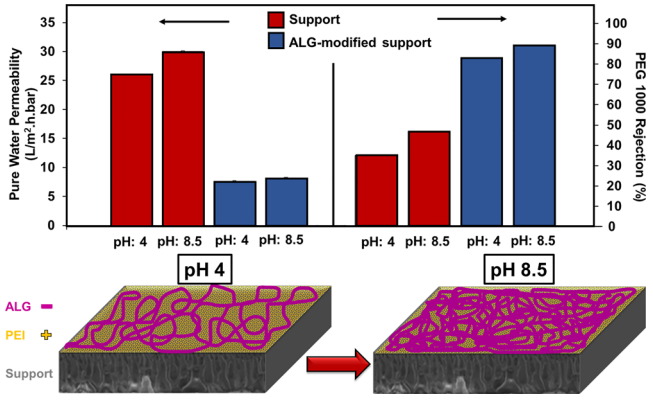


**Figure 3.** Effects of solution pH on the performance of the support and ALG-modified support membranes at 25 °C and schematic of pH-responsive behavior of ALG-modified support membrane.

confirmed by the decrease in the contact angle value from 72.1 ± 0.9 to 67.4 ± 1.0 (Table 2).

Second, the pore size of the membrane decreased because of less repulsion between the chains as a result of fewer ionizable groups of PEI at pH 8.5.[21] Similarly, for the ALG-modified support, an increase in both PWP and PEG 1000 rejection was observed upon altering the pH from 4 to 8.5. Compared to pH 4, ALG is highly charged at pH 8.5 and makes more charge−charge interactions with excess amine groups of PEI. As shown in schematic of Figure 3, this resulted in a thinner and denser layer formation and leads to increased rejection and permeability. The change in rejection capacity of the membrane in solution of varying pH was eliminated after the PBC coating.

Figure 4a demonstrates that the PEG 1000 rejection of the PBC-coated TFC membrane remained constant at ∼89% over the pH range of 4−8.5 while the PWP increased from 13.0 ± 0.63 to 15.9 ± 0.06 L/m$^2$·h·bar. The increase in permeability can be attributed to the enhanced hydrophilic character of the surface (Table 2). The surface became more hydrophilic at pH 8.5 because of the adsorption of $OH^-$ molecules which come from dissociation of NaOH used for adjusting pH to 8.5.



DOI: 10.1021/acsami.9b10273
ACS Appl. Mater. Interfaces 2019, 11, 31367−31377

**Table 2. Contact Angle Values of Support and PBC-Coated TFC Membranes**

| | contact angle measurements | | | |
|---|---|---|---|---|
| | *T*: 4 °C | *T*: 25 °C | pH: 4 | pH: 8.5 |
| membrane code | pH: 7.6 | pH: 7.6 | *T*: 25 °C | *T*: 25 °C |
| support membrane | 65.3 + 1.9 | 66.4 + 1.8 | 72.1 + 0.9 | 67.4 + 1.0 |
| ALG-modified support membrane | 65.2 + 1.4 | 68.0 + 1.7 | 61.0 + 0.9 | 63.4 + 1.4 |
| PBC-coated TFC membrane | 51.2 + 1.6 | 68.7 + 1.8 | 69.8 + 2.1 | 61.7 + 1.1 |

Stable rejection value of the PBC-coated TFC membrane can be explained by the no change in the charge density of the surface with pH (Table 1) which then narrows the number of possible chain conformations (schematic of Figure 4a). Similarly, previous studies have shown that in the presence of a strong polyelectrolyte on the surface, the membrane separation performance remained constant in solutions of varying pH.[14,25,26]

The increase in the permeability of synthetic membranes is usually accompanied by a decrease in the rejection capacity, which is known as the tradeoff between the permeability and selectivity. Most of the efforts in literature have focused on improving the permeability of the membranes without sacrificing the rejection capacity. The results in Figure 4b suggest that our membrane design allowed control of the tradeoff between permeability and rejection. Upon increasing the solution temperature from 4 to 25 °C, the permeability increased by a factor of 2 from 6.7 ± 0.00 to 13.9 ± 0.07 L/m$^2$·h·bar while the PEG 1000 rejection remained constant at ∼89%. This can be explained by the conformational change of the chains only in the vertical direction as a result of a very high grafting density (schematic of Figure 4b).

At low grafting densities ($\sigma$), the responsiveness of the polymer chain approaches that in solution because of the lack of strong interactions between the chains.[27] On the other hand, at high grafting densities, the grafted chains become sterically hindered and, as a result, can only display a vertical conformational change and are unable to undergo a lateral conformational change. We hypothesized that high grafting density of the PBC chains resulted only in a decrease or increase in height of the brushes (schematic of Figure 4b) as a response to temperature. In order to prove our hypothesis about no lateral conformation change of the chains, the average

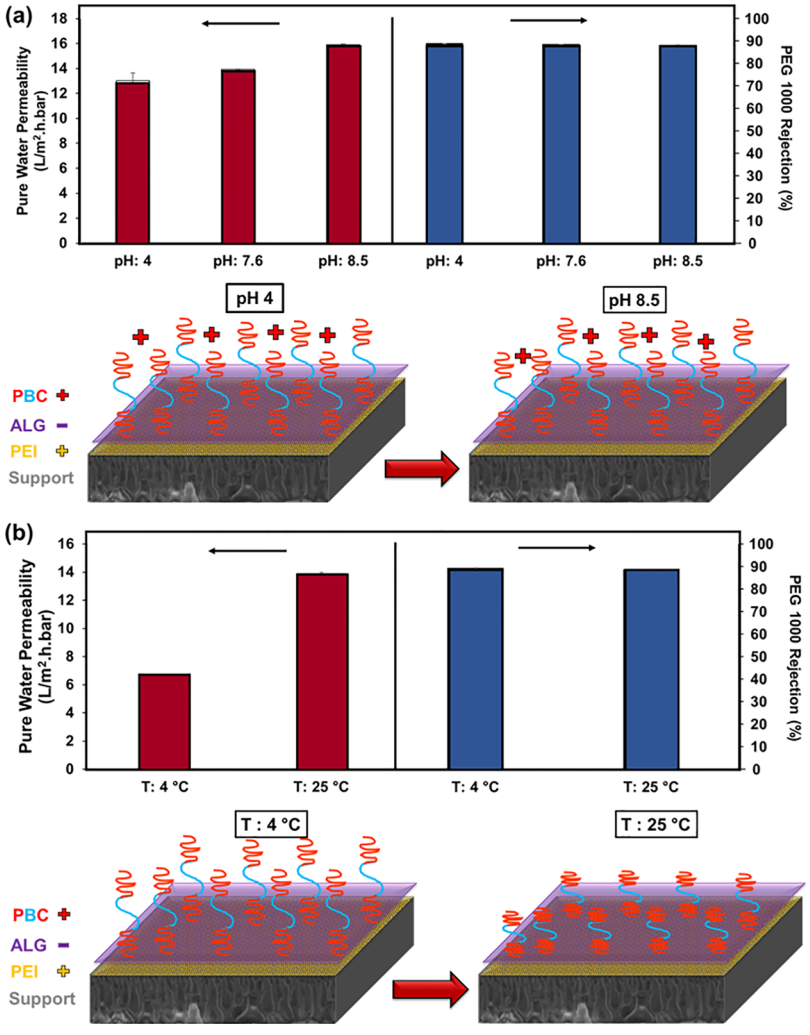


**Figure 4.** (a) Effect of solution pH on the performance of the PBC-coated TFC membrane at 25 °C and schematic of the pH-responsive behavior of the PBC-coated TFC membrane. (b) Effect of solution temperature on the PWP and PEG 1000 rejection of the PBC-coated TFC membrane at pH 7.6 and schematic of the temperature-responsive behavior of the PBC-coated TFC membrane.



DOI: 10.1021/acsami.9b10273
ACS Appl. Mater. Interfaces 2019, 11, 31367−31377

**Scheme 2. Polymer Chain (a) in Solution, Grafted on a Surface in (b) Mushroom configuration and (c) Brush configuration**

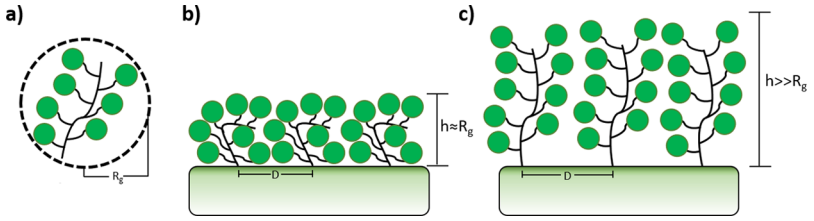


distance between the grafted chains ($D = (1/\sigma)^{0.5}$) was estimated along with the spacing needed to accommodate the unperturbed coils on the surface [$D_{over} = (\pi R_g^2)$][28] (see Scheme 2). Using the experimentally measured grafting density (0.75 mg/cm$^2$) and the radius of gyration value ($R_g$: 20.35 Å) calculated using the small-angle X-ray scattering data (Figure S3 in the Supporting Information Section),[16] the ratio of $\gamma = D/D_{over}$ was found to be very small ($\sim 10^{-3}$). This simply indicated that the PBC chains on the surface were in brushed conformation and the distance between the chains was very small, which supports our hypothesis on the vertical but not lateral conformation of the chains in the presence of external stimuli.

As shown in schematic of Figure 4b, the PBC chains below the LCST (4 °C) became hydrated to form stretched/brush conformations, while the chains above the LCST (25 °C) formed a collapsed structure. Consequently, a thinner layer formed at 25 °C, resulting in higher permeability. This was proved with reflectometry measurements, which demonstrated that the PBC layer on the silicon wafers responded to temperature changes; the brush heights decreased from 557 nm at 4 °C to 337 nm at 25 °C. Temperature responsiveness of the PBC-coated membrane was also demonstrated with AFM images in Figure 5. The membrane showed a roughness

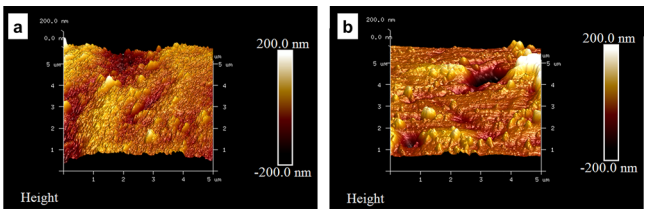


**Figure 5.** AFM images of PBC-coated TFC membranes (a) at *T*: 4 °C below the LCST and (b) at *T*: 25 °C above the LCST.

of $R_a$ = 16.6 nm and $R_q$ = 21.2 nm at 4 °C and $R_a$ = 23.6 nm and $R_q$ = 45.6 nm at 25 °C. As can be seen from Figure 5b, the increase in roughness above the LCST of the PBC occurred due to hydrophobic polymer aggregates induced by the shrinkage of the PBC chains, which is also responsible for an increase in the flux after PBC coating on the ALG-modified support (Figure 4a). The remarkable topography change as a response to temperature was also seen with a maximum vertical distance between the highest and lowest data points in the images measured as 150 and 414 nm at 4 and 25 °C, respectively. Contact angle measurements also proved the temperature responsiveness of the PBC-coated membrane. At pH 7.6, the contact angle of the coated membrane increased from 51.2 ± 1.6 to 68.7 ± 1.8° upon raising the temperature from 4 (<LCST) to 25 °C (>LCST). In contrast, the support and alginate-modified support displayed a negligible difference in the contact angle at 4 and 25 °C (Table 2) because both membranes do not contain any temperature-responsive groups. The changes in contact angle with temperature are a typical behavior observed for other temperature-responsive polymers as well. For example, Takei et al.[29] reported that the contact angle of poly(iV-isopropylacrylamide) (PIPAAm) (LCST: 32 °C) grafted surface decreased from ∼75° to 50° as the temperature changed from 36 °C (>LCST) to 16 °C (<LCST). Below the LCST, polymer chains expand into a rough hydrophilic state while above the LCST chains collapse into a smooth hydrophobic state. Although the surface was more hydrophilic at 4 °C than at 25 °C as confirmed by contact angle measurements (Table 2), the increase in permeability above the LCST (Figure 4b) indicated that the thickness of the selective layer rather than the hydrophilicity of the surface determined the effect of increased solution temperature on the permeability.

Figure 6a shows that the PBC-coated membrane exhibited a step change-like MWCO curve, indicating high selectivity for the solutes that are only 7.8 Å different in terms of their hydrated size. Neutral solutes were selected to determine the MWCO value of the membrane because the rejection of charged solutes is governed both by Donnan exclusion and size exclusion. The rejection of various solutes with molecular weights ranging from 92 to 6000 Da did not change with solution pH or temperature.

Figure 6b illustrates the change in the MWCO and average pore size of the membranes as a function of filtration pH. The pore sizes were predicted by combining the rejection data collected with different-sized solutes and the mathematical model shown in eq 4 through 8. The MWCO and pore radius of the membrane at pH 4.0 was 1161 Da and 0.822 nm, and the corresponding values were 1331 Da and 0.94 nm at pH 8.5 (temperature: 25 °C). When the filtration temperature was raised from 4 °C (<LCST) to 25 °C (>LCST), the MWCO and the pore radius of the membrane were determined to be 1185 Da, 0.826 nm and 1258 Da, and 0.891 nm, respectively. These pore radii are lower than those reported for block co-polymer-based membranes.[13,14] In contrast to our findings, literature studies have shown an increase in the flux accompanied by a decrease in the rejection or MWCO of the membranes when the temperature was increased. For example, Ben Amar et al.[30] reported a decrease in glycerine rejection by the commercial membrane, DESAL5DK, from 27 to 7% by increasing the temperature from 3 to 50 °C. Sharma et al.[31] tested two commercially available polyamide thin-film composite membranes designated as "DL" (Osmonics) and "TFCS" (Koch Fluid Systems) by the respective manufacturers. They reported large increases in MWCO for both membranes (∼100% for DL and 45% for TFCS) when temperature was increased from 5 to 41 °C. The changes in the pore size and MWCO were attributed to the conformational changes of the chains. In light of the literature findings, we can conclude that no change in MWCO and pore size of the



DOI: 10.1021/acsami.9b10273
ACS Appl. Mater. Interfaces 2019, 11, 31367−31377

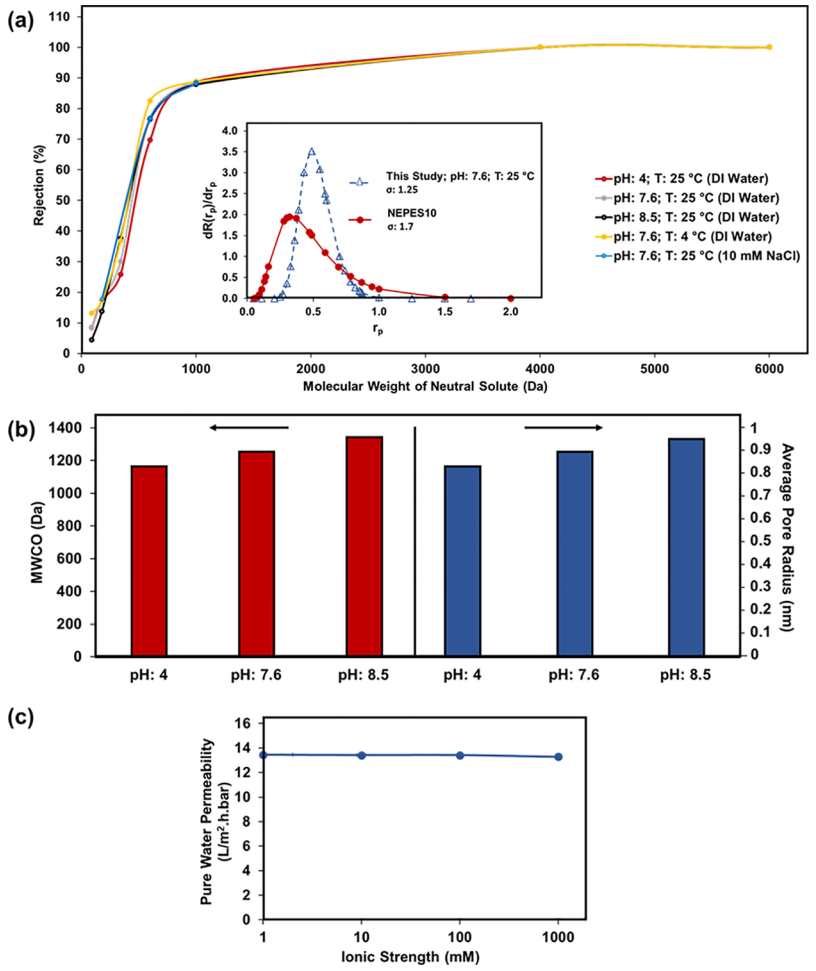


**Figure 6.** (a) Influence of solution pH and temperature on the rejection capacity of the PBC-coated TFC membrane. (b) Effect of solution pH on the MWCO and average pore radius properties of the PBC-coated TFC membrane. Temperature: 25 °C. (c) Change of PWP of the PBC-coated TFC membrane as a function of ionic strength.

**Table 3. Permeability of Commercial NF Membranes**

| supplier | membrane code | membrane material | MWCO (Da) | permeability (L/m$^2$·h·bar) | reference |
|---|---|---|---|---|---|
| GE Osmonics | CK | cellulose acetate | ~2000 | 3.45 | 36 |
| | GE | composite polyamide TFC | 1000 | 1.11 | 37 |
| | GH | polyamide TFC | 2000 | 3.29 | 37 |
| | NDX | polyamide TFC | ~500−700 | 7.9−10.1 | 36 |
| Microdyn Nadir | NP010 | PES | ~1000 | >5 | 38 |
| | NP030 | PES | ~500 | >1 | 38 |
| | N30F | permanently hydrophilic PES | 400 | 3.8 | 39 |
| | TriSep SBNF | cellulose acetate | 2000 | 12−17.7 | 40 |
| | NFPES10 | permanently hydrophilic PES | 1000 | 15.4 | 39 |
| Nitto Denko | NTR7450 | sulfonated PES | 600−800 | 5.7 | 39 |
| sartorius | | | 1000 | 2.55 | 41 |
| this study | PBC coated | PDEAEM-Pluronic F127-PDEAEM | 1000 | 13.0 ± 0.63−15.9 ± 0.06 ($T$: 25 °C) | |

membranes with temperature (or with pH) confirms our hypothesis that the chains do not display any lateral conformation change. The separation ability of the PBC-coated TFC membrane was not compromised in the presence of 10 mM NaCl. As can be seen in Figure 6a, the rejections of glucose, PEG 600, and PEG 1000 dissolved either in DI water or in NaCl were found to be the same. Furthermore, the PWP of the membrane remained constant by changing the ionic strength of the solution from 0 mM up to 1000 mM (Figure 6c), which confirmed that salt ions did not lead to chain rearrangement. Such performance is highly desirable for purely size-based separations. Conformational changes of polymer chains resulting from external stimuli make the membranes less competitive candidates for sharp size-selective separations.[32−35] Zhang et al. reported that the PI−PS−PAA membrane demonstrated significant pH responsiveness and hysteresis, and its rejection capacity decreased in the presence of 10 mM $MgCl_2$.[14] To eliminate the responsiveness of the chains, the membrane needed to go through a series of treatments. First, the PI−PS−PDMA-based support membrane


DOI: 10.1021/acsami.9b10273
ACS Appl. Mater. Interfaces 2019, 11, 31367−31377

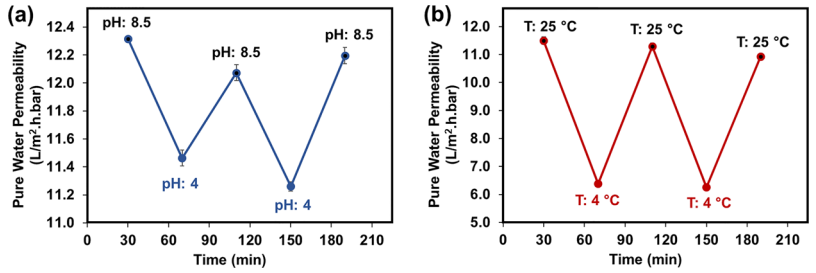


**Figure 7.** Reversible changes of PWP of the PBC-coated TFC membrane as a function of (a) pH and (b) temperature.

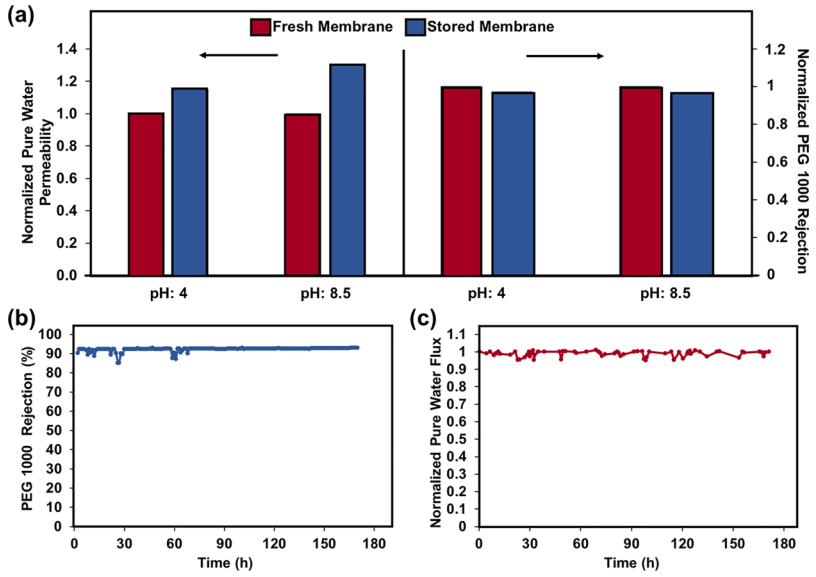


**Figure 8.** (a) Stability of the PBC-coated TFC membrane in terms of PWP and PEG 1000 rejection. Storage time: 30 days. Storage temperature: 25 °C. Long-term stability of the PBC-coated TFC membrane, (b) PEG 1000 rejection, and (c) pure water flux.

was immersed in a 6 M HCl solution at 80 °C for 28 h; next, the sulfonic acid moieties were covalently attached. Although the performance of the resulting membrane (PI−PS−PADSA) did not change in the presence of the external stimuli, lengthy post-treatment procedures, and large amount of co-polymer needed for production limit the use of these membranes for small volume separations. Our membrane also showed robust performance in the presence of external stimuli, pH, temperature, and ionic strength. This can be attributed to the high density of grafted chains in brushed conformation, which was easily achieved by choosing the suitable pH and concentration of the coating solution. In contrast to the previous studies, in our study, no post-treatment was needed in order to access pore sizes below 1 nm.

Table 3 lists the permeability of the commercial membranes with a MWCO value between 500 and 2000 Da. Our membrane has a significantly higher permeability than the 1 kDa (GE, NP010, Sartorius) and even 2 kDa commercial membranes (CK and GH) and a similar permeability with the commercial membrane designated as NFPES10. However, it has a narrower pore size distribution than the NFPES10 (MWCO: 1 kDa), shown as an inset in Figure 6a. The pore size distribution of NFPES10 was predicted based on the rejection data reported in the study of Boussu et al.[39]

**Stability of the Membranes.** The reversibility of the chain responsiveness was determined by measuring PWP through alternately switching the solution pH between 4.0 and 8.5 and solution temperature between 4 and 25 °C. The results shown in Figure 7a,b demonstrated that the permeability immediately changed and was completely reversible upon switching pH and temperature, which confirmed that the conformational change of PBC is reversible.

The pH stability of the membranes is a critical issue for their long-term usage. This was evaluated by storing the membranes in pure water at pH 4.0 and pH 8.5 for 30 days. As can be seen in Figure 8a, the PWP and PEG 1000 rejection values did not change over 1 month of storage. Furthermore, the long-term stability of the membrane during 1 week of continuous cross-flow running was investigated with 1 g/L of PEG 1000 solution at pH 7.6 through monitoring the permeability and PEG 1000 rejection. Both the rejection and flux remained constant during this long run as shown in Figure 8b,c. This result simply indicated the stability of the deposited PBC layer, which is required for practical applications.

## CONCLUSIONS

A new NF membrane was successfully fabricated using a pH- and temperature-responsive PBC. The fabrication method is simple, combining classical non-solvent-induced phase inversion and dynamic coating without requiring complex synthetic routes. This method was able to yield an NF membrane with a pore radius of 0.9 nm while displaying a sharp MWCO. This was the smallest pore radius reported so far for block co-polymer-based membranes. In the presence of significant external stimuli—pH and temperature—the pore size remained constant while the permeability increased with


DOI: 10.1021/acsami.9b10273
ACS Appl. Mater. Interfaces 2019, 11, 31367−31377

increased stimulus. These observations suggest that this new PBC membrane provides a means for overcoming the tradeoff between permeability and selectivity. A persistent conformation of the chains on the lateral direction was achieved through high grafting density. Increasing temperature from 4 °C (<LCST) to 25 °C (>LCST) significantly improved permeability without changing the MWCO of the membrane in contrast to the literature reports. The temperature responsiveness of the developed membrane was demonstrated with the AFM images' contact angle and brush height measurements below and above the LCST. The strong electrostatic interactions between the co-polymer and support enabled the membrane to display long-term stability in acidic and neutral environments. Selectivity retained over a dynamic range of solution conditions, sharp MWCO, sub-nanometer pore size, and long-term stability make this new NF membrane a promising candidate for size-based separation in the recovery of various valuable compounds.

## ■ ASSOCIATED CONTENT

### Supporting Information

The Supporting Information is available free of charge on the ACS Publications website at DOI: 10.1021/acsami.9b10273.

Characterization of PBC (PDF)

## ■ AUTHOR INFORMATION


### Corresponding Author

*E-mail: sacidealsoy@iyte.edu.tr.

### ORCID

Metin Uz: 0000-0003-0341-9264

Surya K. Mallapragada: 0000-0002-9482-7273

Sacide Alsoy Altinkaya: 0000-0002-7049-7425


### Notes

The authors declare no competing financial interest.

## ■ ACKNOWLEDGMENTS

This study was supported by The Scientific and Technical Research Council of Turkey (TUBITAK, grant number: 115M464).

## ■ REFERENCES


(1) Mohammad, A. W.; Teow, Y. H.; Ang, W. L.; Chung, Y. T.; Oatley-Radcliffe, D. L.; Hilal, N. Nanofiltration membranes review: Recent advances and future prospects. *Desalination* **2015**, *356*, 226−254.

(2) Fried, J. R. *Basic Principles of Membrane Technology*; Marcel Mulder (University of Twente, The Netherlands) Kluwer Academic: Dordrecht, 1996; p 564, $255.00. ISBN 0-7823-4247-X. J. Am. Chem. Soc. 1997, 119 (36), 8582-8582.

(3) Abetz, V. Isoporous block copolymer membranes. *Macromol. Rapid Commun.* **2015**, *36*, 10−22.

(4) Jackson, E. A.; Hillmyer, M. A. Nanoporous Membranes Derived from Block Copolymers: From Drug Delivery to Water Filtration. *ACS Nano* **2010**, *4*, 3548−3553.

(5) Nunes, S. P. Block Copolymer Membranes for Aqueous Solution Applications. *Macromolecules* **2016**, *49*, 2905−2916.

(6) Zhang, Y.; Sargent, J. L.; Boudouris, B. W.; Phillip, W. A. Nanoporous membranes generated from self-assembled block polymer precursors:Quo Vadis? *J. Appl. Polym. Sci.* **2015**, *132*, 41683−41699.

(7) Dorin, R. M.; Phillip, W. A.; Sai, H.; Werner, J.; Elimelech, M.; Wiesner, U. Designing block copolymer architectures for targeted membrane performance. *Polymer* **2014**, *55*, 347−353.

(8) Rangou, S.; Buhr, K.; Filiz, V.; Clodt, J. I.; Lademann, B.; Hahn, J.; Jung, A.; Abetz, V. Self-organized isoporous membranes with tailored pore sizes. *J. Membr. Sci.* **2014**, *451*, 266−275.

(9) Stegelmeier, C.; Exner, A.; Hauschild, S.; Filiz, V.; Perlich, J.; Roth, S. V.; Abetz, V.; Förster, S. Evaporation-Induced Block Copolymer Self-Assembly into Membranes Studied by in Situ Synchrotron SAXS. *Macromolecules* **2015**, *48*, 1524−1530.

(10) Yu, H.; Qiu, X.; Moreno, N.; Ma, Z.; Calo, V. M.; Nunes, S. P.; Peinemann, K.-V. Self-Assembled Asymmetric Block Copolymer Membranes: Bridging the Gap from Ultra- to Nanofiltration. *Angew. Chem., Int. Ed.* **2015**, *54*, 13937−13941.

(11) Diep, J.; Tek, A.; Thompson, L.; Frommer, J.; Wang, R.; Piunova, V.; Sly, J.; La, Y.-H. Layer-by-layer assembled core−shell star block copolymers for fouling resistant water purification membranes. *Polymer* **2016**, *103*, 468−477.

(12) Gu, Y.; Wiesner, U. Tailoring Pore Size of Graded Mesoporous Block Copolymer Membranes: Moving from Ultrafiltration toward Nanofiltration. *Macromolecules* **2015**, *48*, 6153−6159.

(13) Mulvenna, R. A.; Weidman, J. L.; Jing, B.; Pople, J. A.; Zhu, Y.; Boudouris, B. W.; Phillip, W. A. Tunable nanoporous membranes with chemically-tailored pore walls from triblock polymer templates. *J. Membr. Sci.* **2014**, *470*, 246−256.

(14) Zhang, Y.; Mulvenna, R. A.; Qu, S.; Boudouris, B. W.; Phillip, W. A. Block Polymer Membranes Functionalized with Nanoconfined Polyelectrolyte Brushes Achieve Sub-Nanometer Selectivity. *ACS Macro Lett.* **2017**, *6*, 726−732.

(15) Determan, M. D.; Cox, J. P.; Seifert, S.; Thiyagarajan, P.; Mallapragada, S. K. Synthesis and characterization of temperature and pH-responsive pentablock copolymers. *Polymer* **2005**, *46*, 6933−6946.

(16) Determan, M. D.; Guo, L.; Lo, C. T.; Thiyagarajan, P.; Mallapragada, S. K. pH- and temperature-dependent phase behavior of a PEO-PPO-PEO-based pentablock copolymer in aqueous media. *Phys. Rev. E: Stat. Phys., Plasmas, Fluids, Relat. Interdiscip. Top.* **2008**, *78*, 021802.

(17) Determan, M. D.; Guo, P.; Mallapragada, S. K. Supramolecular Self-Assembly of Multiblock Copolymers in Aqueous Solution. *Langmuir* **2006**, *22*, 1469−1473.

(18) Bowen, W. R.; Mohammad, A. W. Characterization and Prediction of Nanofiltration Membrane Performance—A General Assessment. *Chem. Eng. Res. Des.* **1998**, *76*, 885−893.

(19) Deen, W. M. Hindered Transport of Large Molecules in Liquid-Filled Pores. *AIChE J.* **1987**, *33*, 1409−1425.

(20) Lin, J.; Ye, W.; Baltaru, M.-C.; Tang, Y. P.; Bernstein, N. J.; Gao, P.; Balta, S.; Vlad, M.; Volodin, A.; Sotto, A.; Luis, P.; Zydney, A. L.; Van der Bruggen, B. Tight ultrafiltration membranes for enhanced separation of dyes and Na2SO4 during textile wastewater treatment. *J. Membr. Sci.* **2016**, *514*, 217−228.

(21) Curtis, K. A.; Miller, D.; Millard, P.; Basu, S.; Horkay, F.; Chandran, P. L. Unusual Salt and pH Induced Changes in Polyethylenimine Solutions. *PLoS One* **2016**, *11*, No. e0158147.

(22) Database. XPS Element or energy. http://www.lasurface.com/database/elementxps.php (accessed July 30, 2019).

(23) Chembio. http://www.chembio.uoguelph.ca/educmat/chm4400_baker/files/CHEM%20%20%20%20%20%20%204400%20lecture%202.pdf (accessed July 30, 2019).

(24) Wavhal, D. S.; Fisher, E. R. Membrane Surface Modification by Plasma-Induced Polymerization of Acrylamide for Improved Surface Properties and Reduced Protein Fouling. *Langmuir* **2003**, *19*, 79−85.

(25) Bernstein, R.; Antón, E.; Ulbricht, M. UV-photo graft functionalization of polyethersulfone membrane with strong polyelectrolyte hydrogel and its application for nanofiltration. *ACS Appl. Mater. Interfaces* **2012**, *4*, 3438−3446.

(26) Wu, C.; Zhao, L.; Zhang, Y. pH-Responsive nanofiltration membranes based on porphyrin supramolecular self-assembly by layer-by-layer technique. *RSC Adv.* **2017**, *7*, 47397−47406.

(27) Wandera, D.; Wickramasinghe, S. R.; Husson, S. M. Stimuli-responsive membranes. *J. Membr. Sci.* **2010**, *357*, 6−35.

(28) Siqueira, D. F.; Breiner, R.; Stamm, M. Adsorption Behavior of Functionalized Polystyrene-block-Polybutadiene with Randomly Attached Adsorbing Sites. *Langmuir* **1995**, *11*, 1680−1687.
(29) Takei, Y. G.; Aoki, T.; Sanui, K.; Ogata, N.; Sakurai, Y.; Okano, T. Dynamic Contact Angle Measurement of Temperature-Responsive Surface Properties for Poly(N-isopropylacrylamide) Grafted Surfaces. *Macromolecules* **1994**, *27*, 6163−6166.
(30) Ben Amar, N.; Saidani, H.; Deratani, A.; Palmeri, J. Effect of Temperature on the Transport of Water and Neutral Solutes across Nanofiltration Membranes. *Langmuir* **2007**, *23*, 2937−2952.
(31) Sharma, R. R.; Agrawal, R.; Chellam, S. Temperature effects on sieving characteristics of thin-film composite nanofiltration membranes: pore size distributions and transport parameters. *J. Membr. Sci.* **2003**, *223*, 69−87.
(32) Luo, J.; Wan, Y. Effects of pH and salt on nanofiltration—a critical review. *J. Membr. Sci.* **2013**, *438*, 18−28.
(33) Mänttäri, M.; Pihlajamäki, A.; Nyström, M. Effect of pH on hydrophilicity and charge and their effect on the filtration efficiency of NF membranes at different pH. *J. Membr. Sci.* **2006**, *280*, 311−320.
(34) Mocan, M.; Wahdat, H.; van der Kooij, H. M.; de Vos, W. M.; Kamperman, M. Systematic variation of membrane casting parameters to control the structure of thermo-responsive isoporous membranes. *J. Membr. Sci.* **2018**, *548*, 502−509.
(35) Schute, K.; Jansen, F.; Rose, M. Solvent-Responsive and Switchable Nanofiltration Membranes based on Hypercrosslinked Polymers with Permanent Porosity. *ChemNanoMat* **2018**, *4*, 562−567.
(36) Sterlitech Corporation. Nanofiltration Membranes. https://www.sterlitech.com/nanofiltration_nf_membrane_%20mkhsp1905.html (accessed July 30, 2019).
(37) Sterlitech Corporation. Flat Sheet Membranes. Ultrafiltration Membranes https://www.sterlitech.com/flat-sheet-membranes.html#uf (accessed July 30, 2019).
(38) Microdyn Nadir. Nanofiltration and Ultrafiltration. https://www.lenntech.com/products/microdyn.htm?gclid=CjwKCAjw7O_pBRA3EiwA_lmtfsYLcYaI6lvee4JXU3cHsNPQKHC43mzLaOVEXbjUJygiYOBOdW1HfhoCVYMQAvD_BwE (accessed July 30, 2019).
(39) Boussu, K.; Van der Bruggen, B.; Volodin, A.; Van Haesendonck, C.; Delcour, J. A.; Van der Meeren, P.; Vandecasteele, C. Characterization of commercial nanofiltration membranes and comparison with self-made polyethersulfone membranes. *Desalination* **2006**, *191*, 245−253.
(40) TRISEP SBNS Cellulose Acetate (CA) NF Membrane. https://static1.squarespace.com/static/54e2b7aee4b0902efd671f90/t/5bc8c9d2652dea19ff740644/1539885522798/SBNF+Flat+Sheet+Membrane.pdf (accessed July 30, 2019).
(41) Bengani, P.; Kou, Y.; Asatekin, A. Zwitterionic copolymer self-assembly for fouling resistant, high flux membranes with size-based small molecule selectivity. *J. Membr. Sci.* **2015**, *493*, 755−765.


DOI: 10.1021/acsami.9b10273
*ACS Appl. Mater. Interfaces* 2019, 11, 31367−31377